Cellular/Molecular

Distribution of Postsynaptic Density (PSD)-95 and Ca^{2+}/Calmodulin-Dependent Protein Kinase II at the PSD

Jennifer D. Petersen,[1] Xiaobing Chen,[1] Lucia Vinade,[1] Ayse Dosemeci,[2] John E. Lisman,[3] and Thomas S. Reese[1]

[1]Laboratory of Neurobiology, National Institute of Neurological Disorders and Stroke, National Institutes of Health, Bethesda, Maryland 20892, [2]Program in Molecular Physiology, Marine Biological Laboratory, Woods Hole, Massachusetts 02543, and [3]Volen Center for Complex Systems, Brandeis University, Waltham, Massachusetts 02454

Postsynaptic densities (PSDs) contain proteins that regulate synaptic transmission. We determined the positions of calcium/calmodulin-dependent protein kinase II (CaMKII) and PSD-95 within the three-dimensional structure of isolated PSDs using immunogold labeling, rotary shadowing, and electron microscopic tomography. The results show that all PSDs contain a central mesh immediately underlying the postsynaptic membrane. Label for PSD-95 is found on both the cytoplasmic and cleft sides of this mesh, averaging 12 nm from the cleft side. All PSDs label for PSD-95. The properties of CaMKII labeling are quite different. Label is virtually absent on the cleft sides of PSDs, but can be heavy on the cytoplasmic side at a mean distance of 25 nm from the cleft. In tomograms, CaMKII holoenzymes can be visualized directly, appearing as labeled, tower-like structures reflecting the 20 nm diameter of the holoenzyme. These towers protrude from the cytoplasmic side of the central mesh. There appears to be a local organization of CaMKII, as judged by fact that the nearest-neighbor distances are nearly invariant over a wide range of labeling density for CaMKII. The average density of CaMKII holoenzymes is highly variable, ranging from zero to values approaching a tightly packed state. This variability is significantly higher than that for PSD-95 and is consistent with an information storage role for CaMKII.

Key words: **postsynaptic density; CaMKII; PSD; PSD-95; electron microscopy; tomography**

Introduction

The postsynaptic density (PSD), an electron-dense structure directly apposed to the cytoplasmic face of the postsynaptic membrane, is prominent at excitatory glutamatergic synapses. The molecular composition of the PSD has been studied by biochemical analyses of isolated fractions and by immunoelectron microscopy (Kennedy, 2000; Sheng, 2001). Some PSD proteins [e.g., PSD-95 and synapse-associated protein 97 (SAP-97)] bind to NMDA and AMPA channels, presumably anchoring them (Kornau et al., 1995; Leonard et al., 1998). Other PSD proteins, enzymes such as serine/threonine, and tyrosine kinases and phosphatases (Malenka and Nicoll, 1999), are implicated in long-term potentiation (LTP). Although much is known about the proteins comprising the PSD, little is known about their organization within the PSD. Immunogold localization of several PSD proteins reveals a laminar organization of some components (Valtschanoff and Weinberg, 2001). Other work reveals a radial organization of receptors at the PSD (Lujan et al., 1996; Racca et al., 2000).

Here, we combine immunogold labeling and rotary shadowing with electron microscopic (EM) tomography to study the three-dimensional organization of isolated PSDs. The high definition intrinsic to this method makes it possible to observe molecular and supramolecular structures within the PSD. The distributions of two key proteins, PSD-95 and calcium/calmodulin-dependent protein kinase II (CaMKII), are compared. PSD-95 is a prototypical member of the family of scaffolding molecules, known as membrane-associated guanylate kinases (MAGUKS) (Cho et al., 1992; Kistner et al., 1993). PSD-95 is implicated in the localization of NMDA receptors (Kornau et al., 1995) and a host of other molecules at the PSD (Tomita et al., 2001). Because overexpression of PSD-95 enhances synaptic transmission (El-Husseini et al., 2000), as does a targeted mutation (Migaud et al., 1998), PSD-95 possibly has a role in synaptic plasticity.

CaMKII, one of the most abundant PSD proteins, plays a central role in LTP (Lisman et al., 2002). During strong synaptic activity, CaMKII translocates to the PSD (Shen and Meyer, 1999; Dosemeci et al., 2001), where it can optimally detect Ca^{2+} entry through NMDA receptors. Once phosphorylated (Fukunaga et al., 1995; Barria et al., 1997), CaMKII is persistently activated (Miller and Kennedy, 1986), leading to potentiation of AMPA-mediated transmission (Derkach et al., 1999; Shi et al., 1999; Hayashi et al., 2000; Poncer et al., 2002). Pharmacological (Otmakhov et al., 1997) and genetic experiments (Giese et al., 1998) show that CaMKII autophosphorylation is necessary for LTP. Determining the localization of CaMKII and PSD-95 in the PSD should provide insight into several fundamental aspects of synaptic function.

Received June 6, 2003; revised Sept. 3, 2003; accepted Oct. 8, 2003.

This work was supported by National Institute of Neurological Disorders and Stroke Grants RO1 NS-27337 and RO1 NS-35083 (J.L.). We thank Morgan Sheng for providing the antibody to Shank and for useful discussions, John Chludzinski for help with all aspects of the photographic work and measurements, and Susan Cheng, Jim Galbraith, and Carolyn Smith for reviewing this manuscript.

Correspondence should be addressed to Dr. Tom Reese, Building 36, Room 2A-19, National Institute of Neurological Disorders and Stroke, National Institutes of Health, Bethesda, MD 20854. E-mail: tsr@codon.nih.gov.

 0270-6474/03/2311270-09$15.00/0

The immunogold labeling of isolated PSDs makes it possible to compare the composition of different individual PSDs, permitting detection of any substantial synapse-to-synapse variation in the density of labeled molecules. Glutamatergic synapses are known to vary greatly in size and efficacy (Harris et al., 1992; Malinow et al., 1994; Takumi et al., 1999); these variations could underlie changes in synaptic transmission encoding previous experiences of the animal. Thus, it is of interest to determine which molecular components vary between PSDs.

Materials and Methods

Isolation of PSDs. PSD fraction was prepared essentially by the method of Carlin et al. (1980), with some modifications. Sprague Dawley rats (12 weeks old) were decapitated, and the brains were removed quickly. The forebrain was dissected out and white matter was scooped out from the forebrain, leaving mainly cerebral cortex. Within 2 min of decapitation, the brain tissue was homogenized in 0.32 M sucrose, 1 mM $MgCl_2$, and 1 μg/ml leupeptin in 1 mM HEPES, pH 7.0. Homogenates were centrifuged at 1400 × *g* for 10 min. Supernatants were saved and pellets were resuspended in the same solution and centrifuged at 710 × *g* for 10 min. Supernatants from the above two steps were combined and were recentrifuged at 710 × *g* for 10 min. The pellets were again discarded. Supernatants were centrifuged at 13,800 × *g* for 10 min. The resulting pellets (P2) were resuspended in 0.32 M sucrose and fractionated by sucrose density centrifugation. Synaptosomes were collected from the 1/1.25 M sucrose interface and treated with 0.5% Triton X-100. Detergent-insoluble pellets from synaptosomes were further fractionated by sucrose density gradient centrifugation (200,000 × *g*) for 2 hr. Material from the 1.5/2.1 M sucrose interface was treated with 0.5% Triton X-100/75 mM KCl and collected on a 2.1 M sucrose cushion by centrifugation at 200,000 × *g* for 40 min (in some preparations the second Triton X-100 extraction step was omitted to improve the yield). The samples were resuspended in 20 mM HEPES, pH 7.4, and again collected on 2.1 M sucrose by centrifugation at 200,000 × *g* for 30 min. The protein staining profile of the PSD fraction is shown in Figure 1*A*.

Immunocytochemistry of PSD fractions. PSDs were immobilized on 5 mm^2 glass coverslips by incubating each coverslip in a 15 μl drop of PSD fraction (1 mg/ml in 20 mM HEPES, pH 7.3) on a clean Teflon block. Immediately before use, coverslips were washed with concentrated nitric acid, creating a substrate to which randomly dispersed PSDs strongly adhered on contact. After immobilization, samples were labeled with immunogold. The polyclonal CaMKII antibody used was custom-made by Multiple Peptide Systems (San Diego, CA), using a 14 aa peptide corresponding to the calmodulin-binding domain of CaMKII, and was affinity-purified using the peptide (Fig. 1*B* shows the specificity of the antibody). The immunogold labeling was performed using CaMKII antibody (1:200 in 1% BSA in TBS); PSD-95 antibody (1:100 in 1% BSA in TBS; catalog number MA1-046; Affinity Bioreagents, Golden, CO) or Shank1a antibody (1:100 in 1% BSA in TBS; gift from M. Sheng, Massachusetts Institute of Technology, Cambridge, MA) according to the following schedule: rinse in 5 mM HEPES for 15 min, block with 1% BSA in TBS for 60 min, block in 2% fish gelatin (Ted Pella, Redding, CA) in TBS for 30 min, incubate in primary antibody for 60 min, rinse in 0.05% Tween 20 in TBS for 30 min, block with 1% BSA in TBS for 60 min, incubate in secondary antibody for 60 min (10 nm colloidal gold conjugated goat anti-mouse IgG; 1:100 in 1% BSA in TBS; Ted Pella, Redding, CA), rinse in Tween 20 for 30 min, and rinse in 5 mM HEPES for 30 min. Antibody incubations were performed in 15 μl droplets on a Teflon block; coverslips were transferred to 60 ml plastic Petri dishes for other steps. All solutions were pH 7.3. Immunogold-labeled samples were next rinsed for 30 sec in doubly distilled water, mounted on a freezing stage, and rapid frozen with a Life Cell (The Woodlands, TX) Slam Freezing machine. Frozen samples were stored under liquid nitrogen until use. Negligible nonspecific label was present in control experiments lacking primary antibody.

Rotary shadow electron microscopy. Each slam frozen coverslip sample was transferred under liquid nitrogen to a precooled Balzers-301 freeze fracture apparatus (Lichtenstein, Austria) and freeze-dried under high vacuum by increasing the temperature from −110 to −100°C for 60 min, and then to −90°C for 45 min. To create a replica of the freeze-dried PSDs, a 1- to 2-nm-thick layer of platinum was deposited onto the rotating coverslip at a 20° angle, followed by a support layer of carbon, 10–12 nm thick, deposited from a 80° angle. Samples were removed from the Balzers machine, and expeditiously floated in hydrofluoric acid, a glass solvent, to liberate the replica and the attached PSD from the glass surface. The replica was then transferred to distilled water and mounted on Formvar-coated 400 mesh copper grids for viewing and image collection on a Jeol 200CX (Peabody, MA) transmission electron microscope. Because of their high electron density, individual 10 nm colloidal gold particles are clearly visible in the replicas. On occasion, gold particles on the surface of a PSD appear to have a halo resulting from platinum deposited directly onto the layer of secondary antibody that coats each gold particle. Gold particles labeling interior portions of the PSD lacked a platinum halo because the platinum shadow could not access these areas. The density of CaMKII and PSD-95 immunogold label per unit area was counted and calculated for cleft and cytoplasmic surfaces of PSDs. Density of CaMKII label on the cleft and cytoplasmic surfaces of PSDs was further differentiated into label residing within 30 nm of the edge zone versus label residing in the interior zone of the PSD, excluding the 30 nm. Gold particles in illustrations were digitally lightened to make them more visible at low magnification.

Nearest-neighbor analyses of CaMKII label. Nearest-neighbor analyses were performed on 28 images of PSDs with variable CaMKII label densities (number of gold label per unit area) ranging from ~20–80 gold particles per 0.1 μm^2 (see Fig. 5). A program was developed by Dr. David Lange (National Institute of Neurological Disorders and Stroke, Bethesda, MD) in Mathematica (Wolfram Research, Champaign, IL), in which nearest-neighbor distances from every CaMKII gold label were calculated after the centers of gold labels on PSDs were marked and their coordinates were recorded. To test whether CaMKII labels are aggregated, random, or evenly spaced compared with the random distribution, the "convex hull" algorithm was used to form a polygon defined by the gold labels close to the edge of the PSD. A second set of the random dots identical in number to the gold particles was then simulated for 50–100 runs within as well as on the boundary of the convex polygon. The mean nearest-neighbor distances of CaMKII labels was then compared with the mean nearest-neighbor distance of the simulated random dots.

EM tomography and height analysis of gold label. EM tomography series were taken on a Jeol 200CX electron microscope at 120 kV with a bottom-mounted, slow-scan, 14 bit, CCD camera (MultiScan-794, Gatan, Pleasanton, CA). The tilt stage was driven by an external voltage source (Harrison 6824A Power supply, Hewlett-Packard, Palo Alto, CA) in series to a timer switch (Dr. Bruce Smith, National Institute of Mental Health, Bethesda, MD) so that the sample holder rotates with uniform but adjustable angular intervals. Data were collected from −60° to +60° in 1.5–2° increments. The image series was then aligned and three-dimensionally reconstructed with IMOD (Kremer et al., 1996) (University of Colorado, Boulder) and EM3D (Harlow et al., 2001, as developed by U. J. McMahan, D. Ress, M. L. Harlow, A. Stoschek, and R. M. Marshall, Stanford University School of Medicine, Stanford, CA). Typical alignment error (rms) is <1.5 pixels. Selected examples were surface-rendered with EM3D. All data were collected at a magnification of 20,000 or 30,000; corresponding resolutions were 0.87 or 0.56 nm/pixel, respectively. The height positions of immunogold particles were determined from the tomogram of the reconstruction. The glass surface, where shadowed, was well delineated, and the distance between this surface and the center of mass of each immunogold particle was then measured.

Results

Rapidly processed PSDs contain basal levels of CaMKII

PSDs were isolated by conventional protocols (Carlin et al., 1980) involving Triton X-100 extraction (Fig. 1*A*). Particular emphasis was placed on rapid homogenization of the brain tissue after decapitation because previous work has shown that a time-dependent increase in the proportion of CaMKII in the PSD

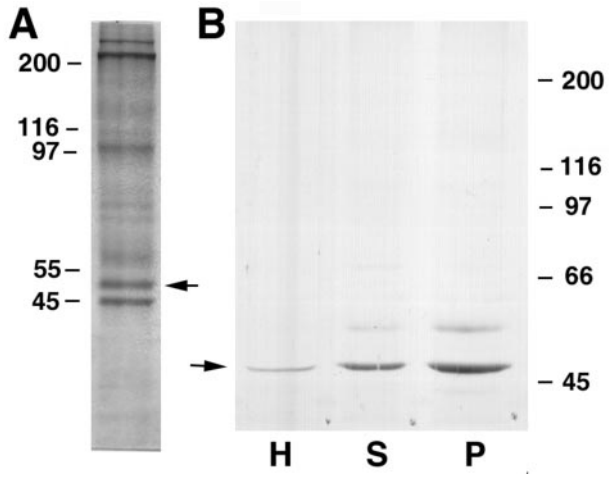

Figure 1. The PSD fraction. *A*, Coomassie blue protein staining profile of the PSD fraction from rapidly processed brains. *B*, Immunoblots with CaMKII antibody of homogenate (H), synaptosome (S), and PSD (P) fractions (10 μg protein each). The antibody recognizes two bands, which correspond to α- and β-CaMKII (α-CaMKII indicated by arrows).

fraction develops in the minutes after decapitation (Suzuki et al., 1994). By extrapolation of this time dependence to zero time, it can be estimated that the basal CaMKII content of the PSD fraction is 2.1%. In this study, protein analysis of PSD fraction prepared from brain tissue homogenized within 2 min of decapitation showed that it contained 2% CaMKII (data not shown). Therefore, it can be concluded that the PSDs we analyzed are close to their average basal CaMKII levels.

Cleft and cytoplasmic surfaces of PSDs differ in structure

Viewed in the electron microscope, replicas of PSDs appeared as distinctive, approximately circular disks ranging in diameter from 180 to 750 nm (mean diameter, 313 ± 4 nm; $n = 618$). These dimensions are consistent with those obtained by serial reconstructions of PSDs at intact synapses (Cohen and Siekevitz, 1978; Harris et al., 1992). Because PSDs are disk-shaped, we expected that they would adhere to the glass substrate in one of two orientations: cleft surface on the glass or cytoplasmic surface on the glass. Only the exposed surface that faced away from the glass would be replicated by rotary platinum shadow, leaving the rest of the PSD invisible, except for any attached immunogold.

PSDs presented two distinct surfaces at approximately equal frequency. One surface was a raised, smooth plateau at a fixed separation from the glass (Fig. 2, left), whereas the other surface had a convoluted contour highly varied in its separation from the glass (Fig. 2, right). These differences in contour were confirmed by examining PSDs in stereo views. Because thin-section views of synapses with prominent PSDs show that the surface of the PSD next to the postsynaptic membrane is planar, whereas the cytoplasmic surface of the PSD extends irregularly into the cytoplasm, it seemed likely that the planar face is the cleft surface, whereas the convoluted face of the PSD is its cytoplasmic surface. Confirmation that the smooth surface of the PSD corresponds to the cleft surface and the convoluted surface to its cytoplasmic aspect is presented below.

The cleft and cytoplasmic surfaces of the PSD were further distinguished by their surface texture. A dense layer of particles, 5–15 nm in diameter, imparting a granular texture, characterized the cleft surface. (Fig. 2*A*,*E*, small arrowheads in *C*) This granular layer covered an underlying lamina composed of 2 nm diameter filaments that formed a central mesh (Fig. 2*C*, small arrow).

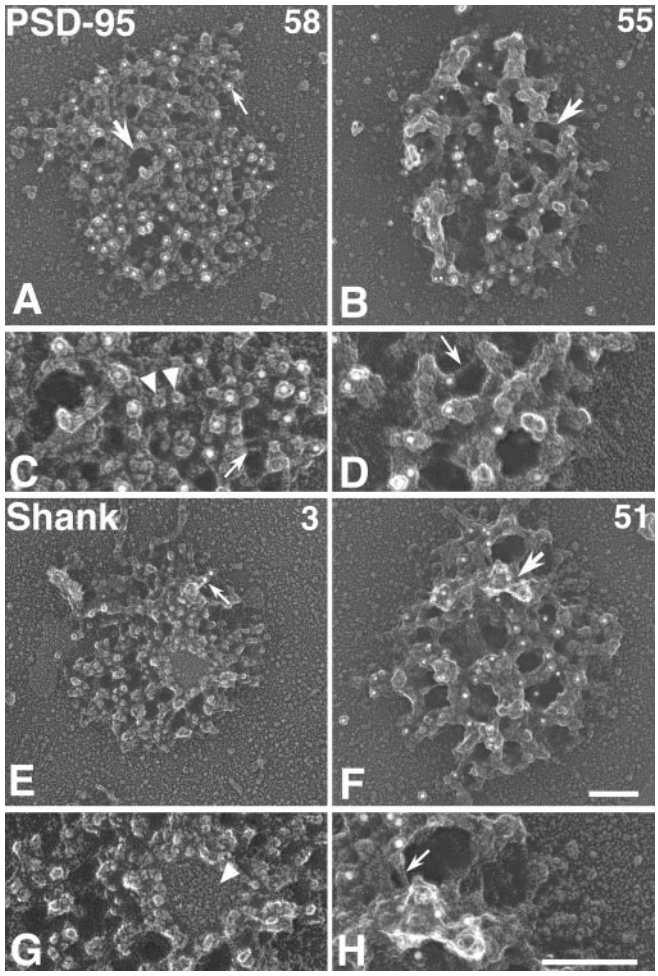

Figure 2. Cleft and cytoplasmic surfaces of PSDs are different. *A*, Cleft surface of PSD immunogold-labeled for PSD-95. Immunogold particles appear as white dots (small arrow). Counts of gold label on PSD are shown at the top right. The opening in the central mesh is indicated by the large arrow. *B*, Cytoplasmic surface of PSD immunogold-labeled for PSD-95. The opening in the central mesh is indicated by an arrow. *C*, Enlarged area from *A*. Granular particles are indicated by arrowheads. Underlying filaments of the central mesh are indicated by an arrow. *D*, Enlarged area of *B*. Underlying filaments of the central mesh are indicated by an arrow. *E*, Cleft surface of PSD immunogold-labeled for Shank. Any label present is typically at edge of PSD (arrow). PSD contains a patch of membrane (enlarged in *G*). *F*, Cytoplasmic surface of PSD immunogold-labeled for Shank. Material protruding above the central mesh is indicated by an arrow. *G*, Membrane patch (arrowhead) has typical rim of particles. *H*, Enlarged area of *F*. Underlying filaments of central mesh are indicated by an arrow. Scale bars, 100 nm.

Openings 40–80 nm in diameter penetrated the central mesh (Fig. 1*A*, large arrow). Patches of membrane 50–100 nm in diameter were frequently observed on the planar surfaces of PSDs, appearing integral to and coplanar with their smooth surfaces. These membranes were typically circular and surrounded by a rim of particles (Fig. 2*E*, arrowhead in *G*, see Fig. 4*C*,*D*). To persist in the isolated PSDs, these membranes must be resistant to Triton X-100 extraction, a characteristic property of the specialized plasma membrane domains known as lipid rafts that are present in synaptosomal preparations (Suzuki, 2002).

In contrast to the planar and granular characteristics of the cleft surface of PSDs, the cytoplasmic surface had a convoluted appearance caused by irregular protrusions from a layer of material covering the central mesh (Fig. 2*B*,*F*). Fine filaments of the central mesh were often visible underlying the protruding material (Fig. 2*D*,*H*, arrows).

Table 1. Distributions of immunogold label on cleft and cytoplasmic sides of isolated PSDs

	Diameter (nm)	Number	Total label (gold/0.1 μm^2)	Distribution (%)
PSD-95				
Cleft	374 ± 23	37	35 ± 2.1	47
Cytoplasmic	335 ± 15	39	37 ± 3.0	53
CaMKII				
Cleft	293 ± 11	57	3.9 ± 0.7	12
Cytoplasmic	358 ± 13	45	28.0 ± 3.2	88
Shank				
Cleft	301 ± 9.0	88	1.7 ± 0.2	10
Cytoplasmic	288 ± 10	57	16 ± 1.9	90

PSDs were labeled with immunogold, and the density ± SEM of gold label was measured in unselected electron micrographs on both cleft and cytoplasmic surfaces of the PSDs. For each antibody, the percentage of label on the cleft and cytoplasmic surfaces was calculated.

Openings in the central mesh were seen more frequently from the cytoplasmic surface than the cleft surface (Fig. 2*B*, arrow), suggesting that the granular layer of the cleft surface covers some openings. Indeed, granular material was visible at the bottom of some openings, but other openings appeared to constitute holes through the PSD, in which case the glass surface was visible at the bottom of an opening. Because platinum was applied at a 20° angle, the protruding material surrounding the openings often blocked platinum from reaching the bottoms of the openings, so it was not always possible to determine whether an opening was a continuous hole through the PSD.

Cleft and cytoplasmic surfaces of PSDs confirmed by protein composition

PSDs attached to glass were labeled with immunogold, freeze-dried, and rotary-shadowed. The distribution of label for various components of the PSD differed on the two surfaces of PSDs. For instance, Shank (Naisbitt et al., 1999), a protein known to lie primarily on the cytoplasmic surface of the PSD by thin-section immunogold-EM (Valtschanoff and Weinberg, 2001) was distributed predominantly on the convoluted surface rather than on the smooth surface (Fig. 2*E,F*, Table 1). The small amount of labeling present on cleft surfaces oriented away from the glass tended to be at the edges (Fig. 2*E*, arrow), and stereo views revealed that this label was actually associated with the convoluted surface of the PSD. Thus, the distribution of label for Shank confirmed that the convoluted surface constitutes the cytoplasmic surface of PSDs and faces the cytoplasm at intact synapses.

PSD-95 label distributed evenly across the central mesh of PSDs

In contrast to Shank, the pattern of immunogold label for PSD-95 was similar on cytoplasmic and cleft surfaces (Fig. 2*A,B*, Table 1). The PSD-95 label followed the contours of the mesh and was present continuously along the mesh. Variability from PSD to PSD was assessed by measuring the density of label per 0.1 μm^2, the area of a typical PSD (Fig. 3). The average density of label was 30 gold particles per 0.1 μm^2 (coefficient of variation = 0.45) for both the cleft and cytoplasmic surfaces of the PSD, and every PSD showed some label. These results indicate that PSD-95 is a component of the central mesh, is accessible to immunogold label from both surfaces of the PSD, and is present in all PSDs.

CaMKII label present exclusively at the cytoplasmic surface

Immunogold labeling for CaMKII showed a pattern of labeling markedly different from that of PSD-95 (Fig. 4). CaMKII immunogold label was seven times heavier on the cytoplasmic surface of the PSD than on the cleft surface (Table 1). The small amount of CaMKII label present on the cleft surface was almost exclusively at the edge of the PSD (Fig. 4*A*, arrows), similar to the edge labeling for Shank. Suspecting that edge labeling is caused by the ability of the antibody to gain access to antigen localized at the edges of the cytoplasmic surface (attached to the glass), the density of label for CaMKII was recomputed after eliminating from consideration a 30 nm wide annular zone at the outer edge of the PSD. After eliminating this potentially distorted edge labeling, the disparity between cleft and cytoplasmic surfaces increased to 40-fold (Table 2). Indeed, when edge label is excluded, the average number of gold particles per unit area on the cleft surface could not be distinguished from the negligible background label on the glass substrate. These results suggest that CaMKII is located exclusively at the cytoplasmic surface of the PSD.

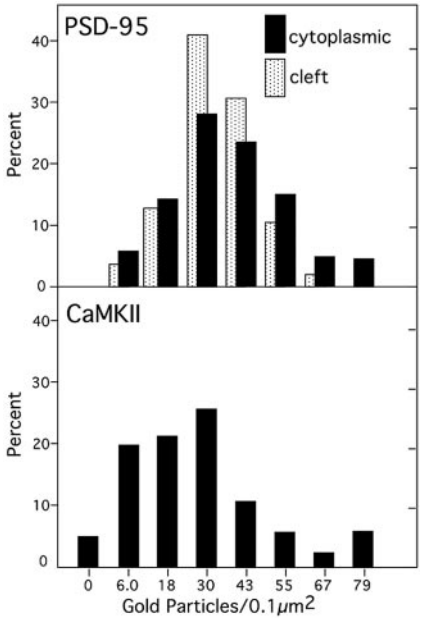

Figure 3. CaMKII immunogold label is concentrated on the cytoplasmic surface of PSDs in variable abundance. Frequency histogram comparing the density of immunogold label for CaMKII and PSD-95 on the cleft and cytoplasmic surfaces of unselected PSDs. Immunogold for PSD-95 is normally distributed on both cleft and cytoplasmic surfaces, whereas essentially all label for CaMKII resides on the cytoplasmic surface, where it varies widely between PSDs. Label for CaMKII on cleft surface is negligible (data not shown)

Density of CaMKII label varies more widely than density of PSD-95 label

The density of CaMKII label on cytoplasmic surfaces appeared to vary dramatically from PSD to PSD (Figs. 3, 4*B,D,F*). Approximately 5% of the PSDs had no gold label and another 20% had only six particles per 0.1 μm^2, whereas all PSDs showed some label for PSD-95. However, 12% of PSDs had >50 particles per 0.1 μm^2 (Fig. 3). The coefficient of variation calculated from the randomly acquired data set (Table 1) for the densities of CaMKII was 0.76, substantially larger than that for the densities of PSD-95 labeling (0.45) (Reed et al., 2002). Based on a labeling efficiency of 0.75 (see below), the CV attributable to probabilistic variation in labeling is small (0.1). An *F* test for comparison of the sizes of the SDs showed that the SD for CaMKII densities was larger than that for PSD-95 densities ($p < 0.005$; both distributions were normalized to their means to allow comparision). We conclude that

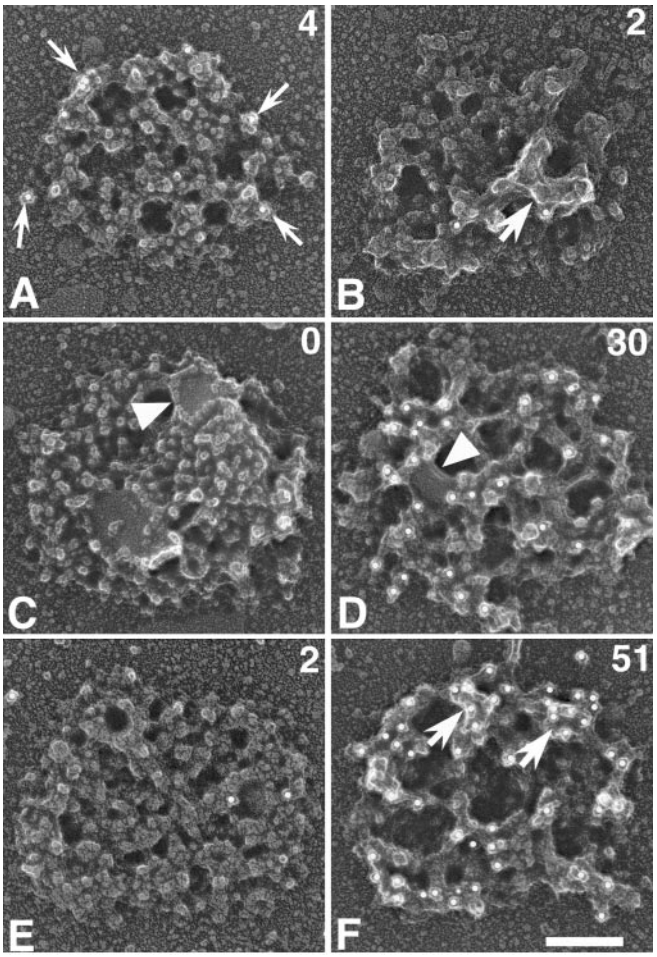

Figure 4. Variable amounts of CaMKII immunogold label are concentrated on cytoplasmic surfaces of PSDs. *A*, Cleft surface of PSD immunogold-labeled for CaMKII. The immunogold label appears as white dots. The label (arrows) is present only at the edge of PSD. The count of gold particles is shown at the top right. *B*, Cytoplasmic surface of PSD immunogold-labeled for CaMKII. The arrow indicates material protruding above the central mesh. *C*, Cleft surface of PSD immunogold-labeled for CaMKII. The arrowhead indicates the membrane patch. *D*, Cytoplasmic surface of PSD with moderate amount of CaMKII immunogold label. A membrane patch lying near the glass substrate is visible from the cytoplasmic surface (arrowhead). *E*, Cleft surface of the PSD showing sparse labeling for CaMKII. *F*, Cytoplasmic surface of a PSD heavily labeled for CaMKII. Arrows indicate concentrated domains of label on protrusions. Scale bar, 100 nm.

Table 2. Distributions of immunogold label for CaMKII on isolated PSDs

			All label	Edge excluded*
	Diameter (nm)	Number	Gold/0.1 μm^2	
Cleft	335 ± 7.6	28	3.0 ± 0.6	0.7 ± 0.3
Cytoplasmic	357 ± 9.0	28	46.0 ± 2.7	31.9 ± 1.9
p value[a]	0.067		0.0001	0.0001

[a]Two-tailed Student's *t* distribution of immunogold label for CaMKII on cleft and cytoplasmic surfaces of a second set of PSDs. Cytoplasmic surfaces of 28 labeled PSDs were compared with an equal number of cleft surfaces of comparable PSDs from the same preparation. The average density of gold particles per unit area (gold/0.1 μm^2 ± SEM) was first determined for the entire surface of each PSD and then for label residing at least 30 nm from the nearest edge of each PSD.

there is substantial variability in the density of CaMKII between PSDs and that this is greater than the variability of PSD-95.

CaMKII label concentrates in subregions of PSDs with a regularity of spacing insensitive to average density

In addition to inter-PSD variability in the amount of CaMKII label present on cytoplasmic surfaces, there also existed an intra-PSD variation in density of label for CaMKII. CaMKII was often concentrated in subregions of a PSD, whereas it was entirely lacking in other regions of the same PSD. Regions that did not label for CaMKII typically lacked material protruding from the central mesh (Fig. 5*C*, asterisks). Hence, the densities of label across the entire cytoplasmic surface of the PSD supplied no information about local densities within individual PSDs. To study local spacing, nearest-neighbor analyses of the distances between immunogold particles within individual PSDs was performed. Histograms of mean nearest-neighbor distances between individual gold particles on a PSD (Fig. 5*A*) showed the peak nearest-neighbor distances. This peak value was then plotted as a function of the average density of label for that PSD (Fig. 5*B*). The peak nearest-neighbor distance (30 ± 5.0 nm) was nearly independent of the average density (Fig. 5*B*). These results suggest that when

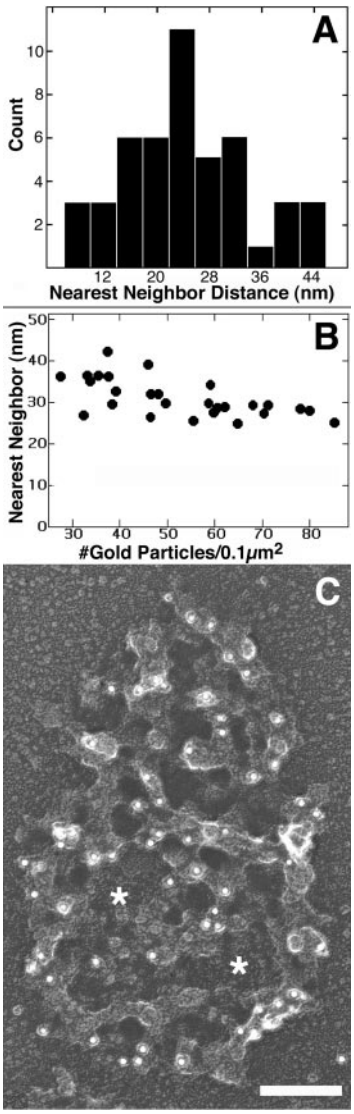

Figure 5. Nearest-neighbor distances between individual labels for CaMKII is independent of label density. *A*, Nearest-neighbor analyses of the distribution of label for CaMKII on typical PSD. Such analyses were performed on 25 representative PSDs in which the density of label varied from 25 to 88 particles per 0.1 μm^2. *B*, Mean nearest-neighbor distances show little variation over a wide range of label densities at 25 PSDs. *C*, PSD in which a large central region has sparse label (asterisks), whereas the rest of the PSD has typically spaced label, illustrating the uniform spacing between label in CaMKII-labeled zones of the PSD. Scale bar, 100 nm.

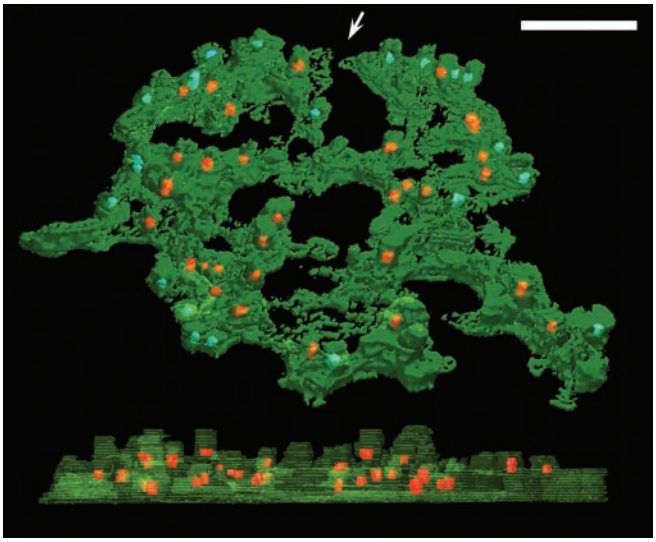

Figure 6. EM tomography shows distribution of CaMKII label in relation to the cleft surface of the PSD. Surface rendering of tomographic reconstruction of a PSD labeled for CaMKII showing an oblique view from the cytoplasmic surface (above) and edge view (below, from aspect indicated by arrow). Centrally located gold particles are labeled in red and shown in the side view. These particles were selected for measurements. Particles in blue, potentially subjected to distortions at edges, were not included in measurements. Scale bar, 100 nm.

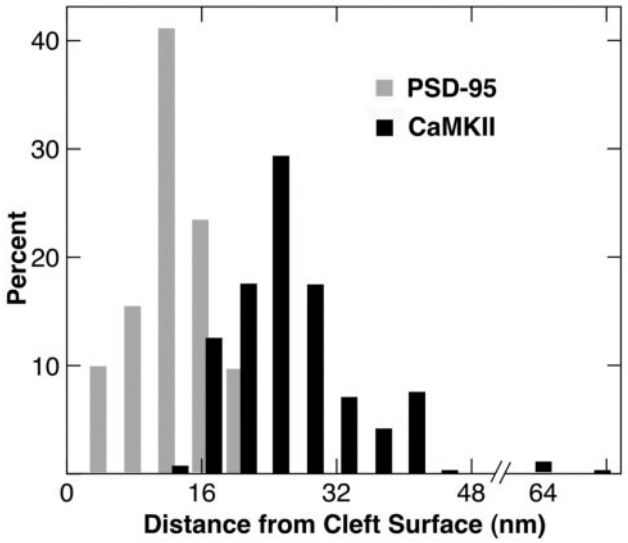

Figure 7. Distinct layering of CaMKII and PSD-95 label detected by EM tomography. Distances of individual gold particles from cleft surfaces of PSDs labeled for PSD-95 or for CaMKII were compared using EM tomography. The distance of individual gold particles from the cleft surface of the PSD, where it adhered to the glass substrate, was measured in nine CaMKII-labeled PSDs and in three PSD-95-labeled PSDs. The density of CaMKII label peaked ~25 nm from the cleft surface of the PSD, whereas the density of PSD-95 peaked at ~12 nm.

present, CaMKII packs at a characteristic local density regardless of overall labeling density.

Thickness of central mesh measured by EM tomography

The thickness of the central mesh in four PSDs that were attached to the glass substrate on their cleft side was measured by EM tomography. Virtual sections cut through the *z*-axis of four PSDs determined that the average thickness of the central mesh was 14 nm, ranging from 11 to 18 nm. Measurement of the thickness of the granular layer was attempted, but it was not possible to differentiate the granular layer from the central mesh confidently, suggesting that the granular layer is exceedingly thin and/or embedded somewhat in the central mesh. Thus, the 14 nm average thickness of the central mesh encompasses the slight contribution to height made by the granular layer.

Distinct layering of CaMKII and PSD-95 label detected by EM tomography

Distances from cleft surfaces of individual gold particles labeling for PSD-95 and CaMKII were compared using EM tomography. Nine complete PSDs labeled for CaMKII (Fig. 6) and three complete PSDs labeled for PSD-95, all adhered to the glass substrate by their cleft surfaces, were reconstructed and compared. Immunogold label (excluding edge label, Table 2) for CaMKII ranged from 14 to 43 nm from the surface of the glass, peaking between 20 and 30 nm (Fig. 7). Thus, essentially all of the CaMKII lies beyond the cytoplasmic surface of the central mesh, which is only 14 nm thick. A small amount of CaMKII label was detected as far as 73 nm from the cleft surface of the PSD. In contrast, immunogold label for PSD-95 peaked at 12 nm from the cleft surface (Fig. 7) and all PSD-95 label lay within 21 nm from the cleft. Thus, PSD-95 should be considered part of the central mesh, whereas CaMKII lies peripheral to it.

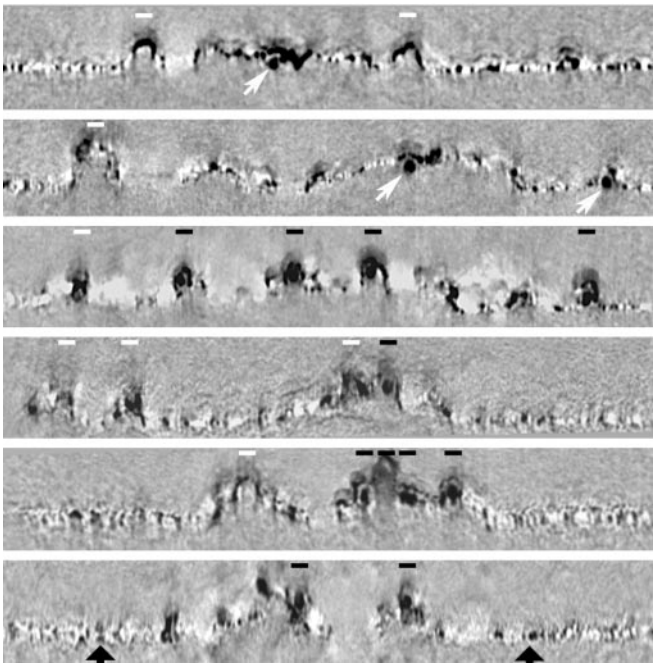

Figure 8. CaMKII immunogold label, but not PSD-95 label, is associated with towers on the cytoplasmic surfaces of PSDs. Cross sections of reconstructions of platinum-shadowed PSDs immunogold-labeled for PSD-95 (top two panels) or CaMKII (bottom four panels). Towers ~20 nm wide (indicated by bars, 20 nm) extend upward from cytoplasmic surfaces of PSDs. After labeling for CaMKII, most towers were labeled (indicated by dark bars), but a few were unlabeled (indicated by white bars). After immunolabeling for PSD-95, towers were unlabeled (white bars), and the label (oblique arrows) was nearer the cleft surface of the PSD. The large black arrows below indicate the plane of the cleft surface on the glass substrate.

CaMKII label associated with tower-like protrusions visualized by EM tomography

EM tomography allowed the visualization of well defined towers with vertical sides among the protrusions of material from the cytoplasmic side of the central mesh (Fig. 8). Towers were typically labeled by a single CaMKII immunogold. Examination of multiple virtual sections (1 nm thick) through reconstructions from four PSDs (including one in Fig. 6) showed that 82% of 152

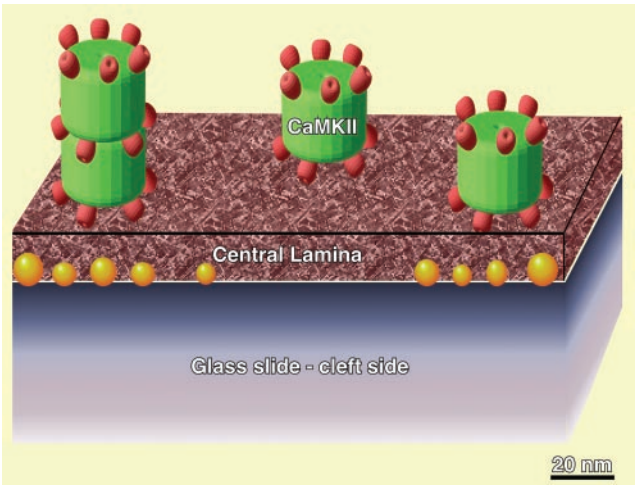

Figure 9. Diagram summarizing structural relationships in isolated PSD. Five holoenzymes (green, catalytic domains in red) are attached to the cytoplasmic side of a small section of a PSD. Three are in a typical cluster and two are stacked end to end. The cleft surface of the central lamina, stripped of the postsynaptic membrane but not of particles (gold), is attached to the glass slide.

towers labeled for CaMKII, and label not associated with towers was <10%. In contrast, no towers labeled for PSD-95 (Fig. 8).

Towers varied in height. In three PSDs examined in virtual serial sections (1 nm thick) through the tomographic reconstructions, the mean height of towers was 34 nm measured from the glass, ranging from 20 to 60 nm. Towers appeared to be ~20 nm in diameter in views generated normal to the plane of the PSD (Fig. 8), consistent with the notion that they represent CaMKII holoenzymes.

Discussion

Multiple lines of evidence indicating the involvement of both CaMKII and PSD-95 in the control of synaptic strength has heightened interest in directly visualizing these molecules within the three-dimensional molecular architecture of the PSD. Here, using immunolocalization and EM tomography, we provide insight into the spatial orientation of PSD-95 and CaMKII within the laminar organization of the PSD. We first highlight the findings, summarized in Figure 9, and then discuss their functional significance.

PSD-95 is a core structural component of central mesh in all PSDs

The cleft surface of the PSD is covered by a thin, densely packed layer of particles, the molecular identity of which remains unclear but of great interest. Immediately underlying the granular cleft layer is the central mesh that in all PSDs labels abundantly for PSD-95. The positioning of PSD-95 close to the cleft surface of the PSD and postsynaptic membrane is consistent with previous work based on thin-section immunogold studies (Valtschanoff and Weinberg, 2001), as well as with the finding that PSD-95 is membrane associated via palmitoylation of its N terminus (Topinka and Bredt, 1998). Furthermore, finding PSD-95 distributed within the central mesh of all isolated PSDs supports the notion that PSD-95 is a fundamental structural component of most, if not all, excitatory PSDs.

Single layer of CaMKII holoenzymes on cytoplasmic side of central mesh

A CaMKII holoenzyme is a 12 subunit, 20-nm-tall barrel-shaped multimer. Catalytic domains of each subunit extend from the top and bottom of the barrel, resulting in a bipolar distribution of catalytic domains (Kolodziej et al., 2000) to which the antibody used in this study is directed. Because the immunogold complexes can define the position of an epitope within ~10 nm, a single layer of CaMKII was expected to give rise to, at most, a 40 nm wide distribution of label. Measured by EM tomography, the average distance of CaMKII label from the cleft surface is ~25 nm. The distance of label from the cleft surface varied from 14 to 43 nm, a range of 29 nm, compatible with the conclusion that most CaMKII holoenzymes reside in a single layer on the cytoplasmic side of the ~14 nm central mesh. However, a small amount of CaMKII label was detected as far as 73 nm from the cleft surface, indicating that some CaMKII may lie in a second, or even third, layer more distal to the postsynaptic membrane (Fig. 9 and below). Such stacking (see below) is consistent with the known ability of CaMKII holoenzymes to self-associate (Hudmon et al., 2001).

Individual CaMKII holoenzymes on cytoplasmic side of the PSD

Virtual sections generated by EM tomography normal to the plane of the PSD made it possible to visualize towers with vertical walls within the convoluted material protruding from the mesh on the cytoplasmic surface of the PSD. The diameter of the towers is close to that of purified CaMKII (Kolodziej et al., 2000) and almost all towers labeled with antibody against CaMKII. The average height of the towers, 34 nm, minus the 14 nm thickness of the central mesh, matches the 20 nm size of CaMKII holoenzymes. However, a few towers were considerably higher, as if two or three barrel-shaped holoenzymes are stacked in register on top of each other. If towers represent single CaMKII holoenzymes, 30–40 holoenzymes could be attached to an average-size PSD. The consistent images of the towers with vertical sides suggests that the cylindrical axis of most molecules is perpendicular to the membrane, as depicted in Figure 8, but we cannot rule out that some holoenzymes lie on their sides on the central mesh.

CaMKII located in variable amounts on cytoplasmic side of PSD

Comparison of the CaMKII labeling among many PSDs indicates that the density of CaMKII gold label can vary from 0 to >75/0.1 μm^2. By comparison, the labeling of PSD-95 is more uniform, as reflected by a lower coefficient of variation and a significantly lower SD. As mentioned above, a typical PSD (0.1 μm^2) contains ~30 CaMKII-labeled molecules on its cytoplasmic surface, but this number varies widely. In fact, 6% of PSDs have a density three times the average and would thus have ~100 holoenzymes attached. Assuming an evenly spaced single layer of kinase, nearest neighbors would be ~30 nm apart. Thus, holoenzymes would be nearly closely packed, leaving only ~10 nm between them. These results imply a large variability in the CaMKII content of PSDs from synapse to synapse. One caveat is that although CaMKII is difficult to extract from the PSD (Kennedy, 1997), the possibility of differential loss of CaMKII from individual PSDs during subcellular fractionation cannot be completely excluded.

CaMKII evenly spaced on cytoplasmic side of PSD

The average nearest-neighbor distance (30 nm) of CaMKII label is nearly independent of the overall density of label. The close, regular spacing of label is apparent over regions of the PSD encompassing many holoenzymes and so cannot be attributed to multiple labeling of single holoenzymes. The factors that enforce this close spacing are unclear. The two known binding proteins

for CaMKII are densin (Walikonis et al., 2001), a protein of unknown function, and the NMDA channel. Importantly, the NMDA channel has a very large cytoplasmic tail that could well be long enough to extend through the central mesh and bind CaMKII (Kennedy and Manzerra, 2001). Recent work shows that under resting conditions, there is a pool of CaMKII complexed with NMDA channels, as determined by coimmunoprecipitation (Gardoni et al., 2001). Thus, the spacing of CaMKII could be dependent on the process that organizes the spacing of NMDA channels. Although many areas of the cytoplasmic surface of the PSD have evenly spaced label for CaMKII, other areas lack label, and in these areas the central mesh is exposed. This higher-order organization of CaMKII within the PSD (some areas evenly labeled, others not labeled) could also reflect the delivery to the PSD of stable packets that contain multiple CaMKII holoenzymes.

Functional consequences of the molecular structure of PSDs

The localization of PSD-95 close to the membrane places it in a position where it can bind to some of its known integral membrane-protein-binding partners. The more distal localization of CaMKII may be related to binding of soluble CaMKII to the PSD induced by neuronal activity. Studies with green fluorescent protein–CaMKII indicate that a pool of the kinase is initially bound to actin at locations distant from the synapse (Shen et al., 1998). Neural activity that elevates Ca^{2+} causes the binding of Ca^{2+}/calmodulin to the kinase, the dissociation of the kinase from actin, the translocation of the kinase to the synaptic region (Shen and Meyer, 1999), specifically to the PSD (Dosemeci et al., 2001), and the binding of the kinase to NMDA channels. Importantly, these processes require enzyme activation but do not require autophosphorylation of the kinase. Once CaMKII is bound to the NMDA channel, it is exposed to the high levels of Ca^{2+} near the NMDA channel that appear to be the trigger for LTP induction. The resulting exposure to sustained high levels of Ca^{2+} near the NMDA channel would favor autophosphorylation of the kinase. Once phosphorylated, CaMKII binds more tightly to the NMDA channel and is persistently active even after Ca^{2+} levels fall. This persistent activity then promotes enzymatic and structural processes that increase the conductance and number of AMPA channels (Lisman et al., 2002). It is these changes that contribute to the enhanced transmission that underlies LTP induction.

The fact that CaMKII binds at high local density is relevant to the mechanism of persistent CaMKII autophosphorylation. The close spacing produces a locally high concentration of phosphorylated sites on the kinase that exceeds the K_m of the PSD phosphatase (PP1) that dephosphorylates CaMKII (Lisman and Zhabotinsky, 2001). The resulting phosphatase saturation should enable CaMKII autophosphorylation activity to keep the molecule phosphorylated and active.

AMPA receptors, like CaMKII molecules, vary greatly in number and density from synapse to synapse. Some synapses, termed silent synapses, lack AMPA receptors, whereas others have high AMPA receptor densities (Nusser et al., 1998, Petralia et al., 1999, Takumi et al., 1999). NMDA channels, in contrast, appear to vary much less (Racca et al., 2000). The variability in AMPA channels is thought to be a factor underlying differences in synaptic strength that reflect the history of synaptic modifications during development and experience (LTP). It has been proposed that persistently phosphorylated CaMKII bound to NMDA channels serves to organize additional anchoring sites for AMPA channels and thereby to strengthen transmission (Lisman and Zhabotinsky, 2001). The variability we have observed in CaMKII density would be consistent with such a role. Therefore, it will be important to determine how the variability in density of CaMKII reported here correlates with the variability in the AMPA receptor content of synapses.

References

Barria A, Muller D, Derkach V, Griffith LC, Soderling TR (1997) Regulatory phosphorylation of AMPA-type glutamate receptors by CaMKII during long-term potentiation. Science 276:2042–2045.

Carlin RK, Grab DJ, Cohen RS, Siekevitz P (1980) Isolation and characterization of postsynaptic densities from various brain regions: enrichment of different types of postsynaptic densities. J Cell Biol 86:831–845.

Cohen RS, Siekevitz P (1978) Form of the postsynaptic density: a serial section study. J Cell Biol 78:36–46.

Cho KO, Hunt CA, Kennedy MB (1992) The rat brain postsynaptic density fraction contains a homolog of the *Drosophila* discs-large tumor suppressor protein. Neuron 9:929–942.

Derkach V, Barria A, Soderling TR (1999) Ca^{2+}/calmodulin-kinase II enhances channel conductance of alpha-amino-3-hydroxy-5-methyl-4-isoxazolepropionate type glutamate receptors. Proc Natl Acad Sci USA 96:3269–3274.

Dosemeci A, Tao-Cheng J-H, Vinade L, Winters C, Pozzo-Miller L, Reese TS (2001) Glutamate-induced transient modification of the postsynaptic density. Proc Natl Acad Sci USA 98:10428–10432.

El-Husseini AE, Schnell E, Chetkovich DM, Nicoll RA, Bredt DS (2000) PSD-95 Involvement in maturation of excitatory synapses. Science 290:1364–1368.

Fukunaga K, Muller D, Miyamoto E (1995) Increased phosphorylation of Ca^{2+}/calmodulin-dependent protein kinase II and its endogenous substrates in the induction of long-term potentiation. J Biol Chem 270:6119–6124.

Gardoni F, Schrama LH, Kamal A, Gispen WH, Cattabeni F, Luca MD (2001) Hippocampal synaptic plasticity involves competition between Ca^{2+}/calmodulin-dependent protein kinase II and postsynaptic density 95 for binding to the NR2A subunit of the NMDA receptor. J Neurosci 21:1501–1509.

Giese KP, Fedorov NB, Filipkowski RK, Silva AJ (1998) Autophosphorylation at Thr286 of the a calcium-calmodulin kinase II in LTP and learning. Science 279:870–873.

Harlow ML, Ress D, Stoschek A, Marshall RM, McMahan UJ (2001) The architecture of active zone material at the frog's neuromuscular junction. Nature 409:479–484.

Harris KM, Jensen FE, Tsao B (1992) Three-dimensional structure of dendritic spines and synapses in rat hippocampus (CA1) at postnatal day 15 and adult ages: implications for the maturation of synaptic physiology and long-term potentiation. J Neurosci 12:2685–2705.

Hayashi Y, Shi S, Esteban JA, Piccini A, Poncer JC, Malinow R (2000) Driving AMPA receptors into synapses by LTP and CaMKII: requirement for GluR1 and PDZ domain interaction. Science 287:2262–2267.

Hudmon A, Kim SA, Kolb SJ, Stoops JK, Waxham MN (2001) Light scattering and transmission electron microscopy studies reveal a mechanism for calcium/calmodulin-dependent protein kinase II self-association. J Neurochem 76:1364–1375.

Kennedy MB (1997) The postsynaptic density at glutamatergic synapses. Trends Neurosci 20:264–268.

Kennedy MB (2000) Signal-processing machines at the postsynaptic density. Science 290:750–754.

Kennedy MB, Manzerra P (2001) Telling tails. Proc Natl Acad Sci USA 98:12323–12324.

Kistner U, Wenzel BM, Veh RW, Cases-Langhoff C, Garner AM, Appeltauer U, Voss B, Gundelfinger ED, Garner CC (1993) SAP90, a rat presynaptic protein related to the product of the *Drosophila* tumor suppressor gene dlg-A. J Biol Chem 268:4580–4583.

Kolodziej S, Hudmon A, Waxham MN, Stoops JK (2000) Three-dimensional reconstructions of calcium/calmodulin-dependent (CaM) kinase II-alpha and truncated CaM kinase II alpha reveal a unique organization for its structural core and function domains. J Biol Chem 275:14354–14359.

Kornau H-C, Schenker LT, Kennedy MB, Seenburg PH (1995) Domain interaction between NMDA receptor subunits and the postsynaptic density protein PSD-95. Science 269:1737–1740.

Kremer JR, Mastronarde DN, McIntosh JR (1996) Computer visualization of three-dimensional image data using IMOD. J Struct Biol 116:71–76.

Leonard AS, Davare MA, Horne MC, Garner CC, Hell JW (1998) SAP97 is associated with the α-amino-3-hydroxy-5-methylisoxazole-4-propionic acid receptor GluR1 subunit. J Biol Chem 273:19518–19524.

Lisman J, Schulman H, Cline H (2002) The molecular basis of CaMKII function in synaptic and behavioural memory. Nat Rev Neurosci 3:175–190.

Lisman JE, Zhabotinsky AM (2001) A model of synaptic memory: a CaMKII/PP1 switch that potentiates transmission by organizing an AMPA receptor anchoring assembly. Neuron 31:191–201.

Lujan R, Nusser Z, Roberts JD, Shigemoto R, Somogyi P (1996) Perisynaptic location of metabotropic glutamate receptors mGluR1 and mGluR5 on dendrites and dendritic spines in the rat hippocampus. Eur J Neurosci 8:1488–1500.

Malenka RC, Nicoll RA (1999) Long-term potentiation: a decade of progress? Science 285:1870–1874.

Malinow R, Otmakhov N, Blum KI, Lisman J (1994) Visualizing hippocampal synaptic function by optical detection of Ca^{2+} entry through the *N*-methyl-D-aspartate channel. Proc Natl Acad Sci USA 91:8170–8174.

Migaud M, Charlesworth P, Dempster M, Webster LC, Watabe AM, Makhinson M, He Y, Ramsay M, Morris R, Morrison JH, O'Dell TJ, Grant SGN (1998) Enhanced long-term potentiation and impaired learning in mice with mutant postsynaptic density-95 protein. Nature 396:433–439.

Miller SG, Kennedy MB (1986) Regulation of brain type II Ca^{2+}/calmodulin-dependent protein kinase by autophosphorylation: a Ca^{2+}-triggered molecular switch. Cell 44:861–870.

Naisbitt S, Kim E, Tu J, Xiao B, Sala C, Valtschanoff J, R. J., W., Worley PF, Sheng M (1999) Shank, a novel family of postsynaptic density proteins that binds to the NMDA receptor/PSD-95/GKAP complex and cortactin. Neuron 23:569–582.

Nusser Z, Lujan R, Laube G, Roberts JD, Molnar E, Somogyi P (1998) Cell type and pathway dependence of synaptic AMPA receptor number and variability in the hippocampus Neuron 21:545–559.

Otmakhov N, Griffith LC, Lisman JE (1997) Postsynaptic inhibitors of calcium/calmodulin-dependent protein kinase type II block induction but not maintenance of pairing-induced long-term potentiation. J Neurosci 17:5357–5365.

Petralia RS, Esteban JA, Wang YX, Partridge JG, Zhao HM, Wenthold RJ, Malinow R (1999) Selective acquisition of AMPA receptors over postnatal development suggests a molecular basis for silent synapses. Nat Neurosci 2:31–36.

Poncer JC, Esteban JA, Malinow R (2002) Multiple mechanisms for the potentiation of AMPA receptor-mediated transmission by α-Ca^{2+}/calmodulin-dependent protein kinase II. J Neurosci 22:4406–4411.

Racca C, Stephenson FA, Streit P, Roberts JDB, Somogyi P (2000) NMDA receptor content of synapses in stratum radiatum of the hippocampal CA1 area. J Neurosci 20:2512–2522.

Reed GF, Lynn F, Meade BD (2002) Use of coefficient of variation in assessing variability of quantitative assays. Clin Diagn Lab Immunol 9:1235–1239.

Shen K, Meyer T (1999) Dynamic control of CaMKII translocation and localization in hippocampal neurons by NMDA receptor stimulation. Science 284:162–166.

Shen K, Teruel MN, Subramanian K, Meyer T (1998) CaMKIIβ functions as an F-actin targeting module that localizes CaMKIIα/β heterooligomers to dendritic spines. Neuron 21:593–606.

Sheng M (2001) Molecular organization of the postsynaptic specialization. Proc Natl Acad Sci USA 98:7058–7061.

Shi S, Hayashi Y, Petralia R, Zaman S, Wenthold RJ, Svoboda K, Malinow R (1999) Rapid spine delivery and redistribution of AMPA receptors after synaptic NMDA receptor activation. Science 284:1811–1816.

Suzuki T, Okumura-Noji K, Tanaka R, Tada T (1994) Rapid translocation of cytosolic Ca^{2+}/calmodulin-dependent protein kinase II into postsynaptic density after decapitation. J Neurochem 63:1529–1537.

Suzuki T (2002) Lipid rafts at the postsynaptic sites: distribution, function and linkage to postsynaptic density. Neurosci Res 44:1–9.

Takumi Y, Ramirez-Leon V, Laake P, Rinvik E, Ottersen OP (1999) Different modes of expression of AMPA and NMDA receptors in hippocampal synapses. Nat Neurosci 2:618–624.

Tomita S, Nicoll RA, Bredt DS (2001) PDZ protein interactions regulating glutamate receptor function and plasticity. J Cell Biol 153:F19–F24.

Topinka JR, Bredt DS (1998) N-terminal palmitoylation of PSD-95 regulates association with cell membranes and interaction with K^+ channel Kv1.4. Neuron 20:125–134.

Valtschanoff JG, Weinberg RJ (2001) Laminar organization of the NMDA receptor complex within the postsynaptic density. J Neurosci 21:1211–1217.

Walikonis RS, Oguni A, Khorosheva EM, Jeng CJ, Asuncion FJ, Kennedy MB (2001) Densin-180 forms a ternary complex with the α-subunit of Ca^{2+}/calmodulin-dependent protein kinase II and α-actinin. J Neurosci 21:423–433.